Prod. Eng. Res. Devel. (2008) 2:9–14
DOI 10.1007/s11740-007-0059-z

PRODUCTION PROCESS

Modeling of contact behavior between polishing pad and workpiece surface

Fritz Klocke · Olaf Dambon · Richard Zunke

Received: 29 June 2007 / Accepted: 11 October 2007 / Published online: 27 November 2007

Abstract The polishing pad is one of the most significant components within a polishing system. It influences both the material removal rate and the surface finish. Furthermore, the wear behavior of the polishing pad is responsible for the shape accuracy. Nevertheless despite extensive research activity in recent years, there are still gaps of knowledge in terms of the working principle of a polishing pad. In this paper, the contact behavior of a polishing pad (polyurethane foam) with the workpiece surface is examined. For this, the polishing pad is modeled using a finite-element modeling (FEM) program and the deformation by pressing it against the rigid workpiece surface is investigated. Consequently, the local tensions are calculated, which are the basis for the penetration depth and therefore also for the material removal rate.

Keywords Production process · Polishing · Steel

1 Introduction

The polishing pad with its properties influences the performance of the polishing process and therefore the polishing result. During the process the pad shape and consequently shape deviations caused by wear are imaged to the workpiece surface [1]. In order to realize the required shape accuracy for optical applications, the mechanisms causing pad wear must be understood. Pad wear, however, only takes place when there is a direct contact between the soft pad and the hard workpiece. Therefore, the contact behavior with the workpiece has to be investigated and models focusing on the pad-workpiece interface have to be developed. Based on these models, the working principle of polishing pads can be described and measures reducing pad wear can be derived.

The investigations presented in this paper were carried out within the research project SFB TR/4 funded by the German Research Association, Deutsche Forschungsgemeinschaft (DFG).

F. Klocke · O. Dambon · R. Zunke (✉)
Institute of Machine Tools and Production Engineering,
Aachen University of Technology, Aachen, Germany
e-mail: richard.zunke@ipt.fraunhofer.de

2 Modeling of contact geometries

Tribology theory states that tribological systems consist of active surface areas acting in pairs. In micro geometry terms, when the technical surfaces of two components come into contact with each other, a series of discrete micro contacts can be observed, where deformation takes place due to the normal load F_N. Therefore, it is important to distinguish between the apparent contact area A_0, which can be calculated on the basis of geometrical data, and the actual, much smaller contact area A_r. The real or actual contact area is fundamental to all tribological systems like in this present case of investigation, where friction and wear processes take place (Fig. 1).

When this theory is applied to polishing processes, the contact behavior between the workpiece surface, the polishing pad and the abrasive particles embedded herein become relevant for the process of material removal. The contact geometry determined on the basis of the Theory of Elastic Contact Deformation developed in the nineteenth century by Hertz has been modified by Archard [2], Greenwood and Tripp [3]. In comparison to the rough surface of the polishing pad, the workpiece can be regarded as an ideal smooth surface, in which case the Greenwood–Williamson model can be applied [4]. This theory describes

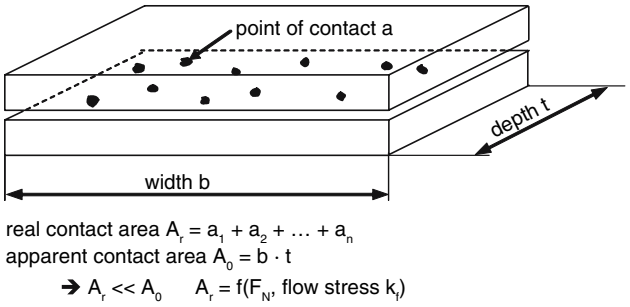

Fig. 1 Contact ratios in the working gap

the contact geometry between a smooth and a rough surface subjected to a normal load F_N. Based on this model, the real contact area A_r can be calculated:

$$A_r = \pi \cdot \chi \cdot A_0 \cdot r_K \cdot \int_u^\infty (h_R - u) \cdot \Phi(h_R) dh_R \qquad (1)$$

In this equation, χ represents the total number of asperities per unit area, A_0 the nominal (apparent) contact area, r_K the mean (average) radius of asperity, h_R the height of asperity, and u the mean (average) distance between rough surface and smooth workpiece surface. The function $\Phi(h_R)$ represents the distribution density function of the asperity ordinate values.

This equation has provided the basis for numerous scientific investigations of the contact behavior as a part of the polishing process [5, 6]. The average local applied pressure p_r can be calculated using the real contact area determined in (1) and

$$p_r = \frac{F_N}{A_r}. \qquad (2)$$

Here, F_N is the normal load applied to the entire surface. Alternatively, FE models can be utilized to simulate the contact behavior of the workpiece.

The FE model is based on a digitized section of the polishing pad topography. The data was gained by using a chromatic sensor mounted on a precise positioning device, which allows a non contact measurement of the surface topography. Subsequently, this data is processed in such a way that it can be entered into the relevant FEM program. Figure 2 shows a section of FEM mesh from a digitalized polishing pad.

First, in order to simulate the contact behavior, the workpiece must be regarded as an ideal rigid and smooth body, while the polishing pad is assumed to have viscoelastic properties. Later, in order to investigate the material stress and deformation caused by the penetrating grains, this restriction will be lifted and the workpiece will be regarded as elastic. When subjected to external

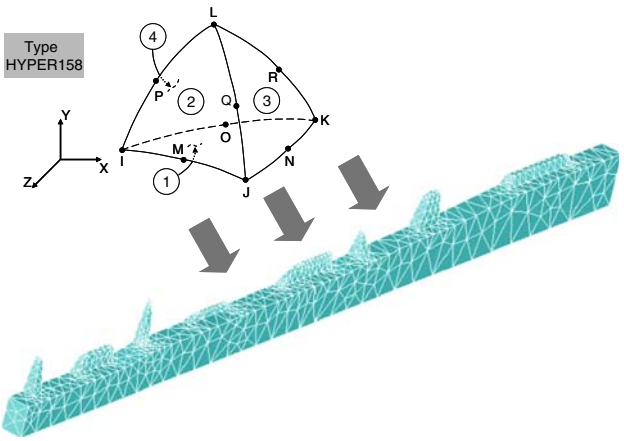

Fig. 2 FE model of a pad surface section using the Hyper158 element

pressure, the internal stress in viscoelastic materials does not increase abruptly as in the case of elastic materials and the stress–strain curve does not correspond to Hooke's Law. Therefore, the Mooney–Rivlin model [7] has to be applied, which is based on the postulation that the energy is independent of the applied coordinate system. These three fundamental invariant strain functions are designated I_1, I_2 and I_3, and represent the length, area and volume respectively ($I_3 = 1$ for an incompressible material). The energy function W_V (required deformation energy) is given by

$$W_V = c_{10} \cdot (I_1 - 3) + c_{01} \cdot (I_2 - 3) + \frac{1}{d_{ic}}(J - 1)^2 \qquad (3)$$

whereby c_{10}, c_{01} represent the material constants describing the deformation, d_{ic} the material incompressibility parameter, and J the determinant of elastic deformation gradient. Furthermore, Young's modulus and Poisson's ratio are needed in order to determine the deformation behavior of the polyurethane pad.

The model illustrated in Fig. 2 and the subsequent contact simulation are used to determine the real contact area in relation to the apparent contact area for two exemplary polishing pads with different Young's Moduli (Fig. 3). This clearly demonstrates that, despite the use of a relatively soft polishing pad in comparison to the hard workpiece surface, the contact area only represents a minute proportion of the apparent area. The real contact area in the example shown here, does not exceed 1% of the apparent contact area despite the relatively high applied pressure (3 bar). Equation (2) also describes the pressure that results in the real contact area. The extremely small contact area leads to the generation of very high-localized surface pressure, far greater than the original globally applied load. The points of high pressure occurring in the contact areas of the polishing pad are responsible for the

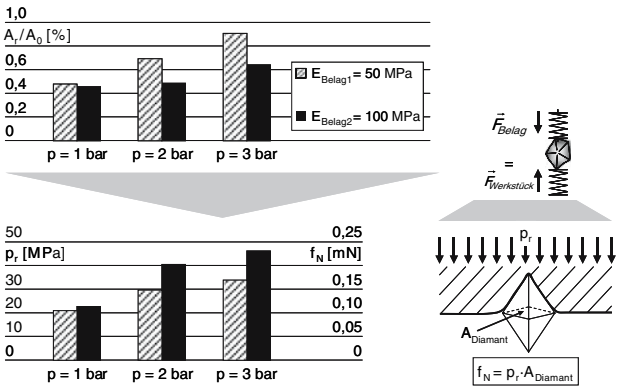

Fig. 3 Relation of A_r to A_0 and p_r to globally applied pressure p for different polishing pads

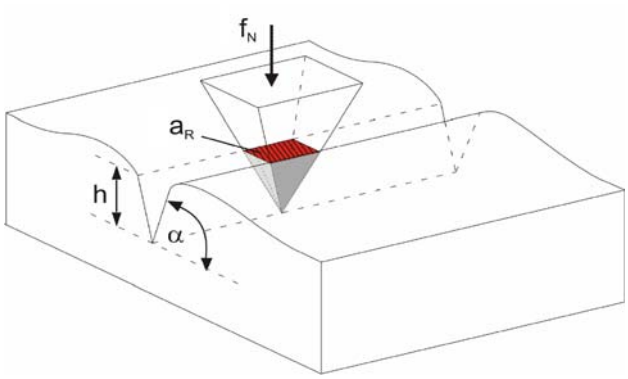

Fig. 4 Model of a penetrating diamond grain

normal forces generated per grain. These ultimately determine the flow stress in the workpiece surface. Figure 3 illustrates the normal forces that occur in a typical 3-µm long pyramid shaped diamond grain. The use of a diamond slurry in combination with polyurethane foam as a polishing pad is based on extensive experiments conducted in order to determine the surface interactions in steel polishing [8].

This model highlights the fact that the external load is fully transmitted into the polishing pad. If polishing grains are present in the contact zone, these are subject to a normal load (Fig. 3). Assuming that the polishing pad is not 'saturated' (i.e., the maximum density of abrasive particles has not been reached), the normal forces depend on the polishing pad properties such as surface topography, roughness and the modulus of elasticity rather than on the number of polishing grains in the contact zone.

It has to be considered that the presented model only applies to static conditions. During the polishing process the surface of the polishing pad is not permanently in contact with the workpiece, but is subject to an alternating load. Under dynamic conditions, both the elastic and the viscous material properties are relevant. The polishing pad in the contact zone is also subject to tribological loads, which in turn changes the surface topography. This dynamic behavior has not been considered by the calculations shown in Fig. 3.

The results for normal load per grain as depicted in Fig. 3 do, however, draw attention to the fact that the normal load is very small in comparison to the globally applied load—it lies within the range of nanoindentation processes. This emphasizes the fact that the material properties on the surface are relevant to the polishing process, not the properties in the material underneath the surface. Furthermore the surface properties can differ significantly from those of the underlying material.

3 Analysis of polishing depth

In order to mechanically remove material from the workpiece, the abrasive particle (here modeled as a rigid pyramid, Fig. 3) must penetrate the surface of the material. This process is driven by the normal load f_N acting on the individual particles, which can be determined through contact modeling and reaches the orders of magnitude depicted in Fig. 5. The polishing depth allows us to estimate the extent of material removal. This depth depends on external factors, such as Young's Modulus for the polishing pad or the applied surface loads (Fig. 3) as well as on the underlying material hardness and grain geometry.

The resistance to a harder object represented by the material hardness is defined as follows:

$$H = \frac{f_N}{a_R} \tag{4}$$

whereby a_R is the cross-sectional area of the penetrating part of the grain. a_R can be used to determine the penetration depth h as a function of the inclination α (Fig. 4).

The compressive stress in the contact area shown in Fig. 3 results in a normal load per grain of approx. 1.0 mN for a polishing pad with a Young's Modulus of $E_{B1} = 50$ MPa. The polishing depths relative to the inclination α, the normal load and the hardness are illustrated in Fig. 5. The material hardness values used here were determined by nanoindentation processes.

It also becomes clear that the inclination of the abrasive particle has the most significant effect on polishing depth while increased hardness or greater normal loads per grain have a relatively small effect. These diagrams also show that the processes relevant to material removal mainly take place within the first 300 nm of the boundary zone. Consequently, the physical and chemical properties of the boundary zone are pivotal to the polishing process. Detailed investigations on the surface interactions in steel polishing were published by Dambon [8].

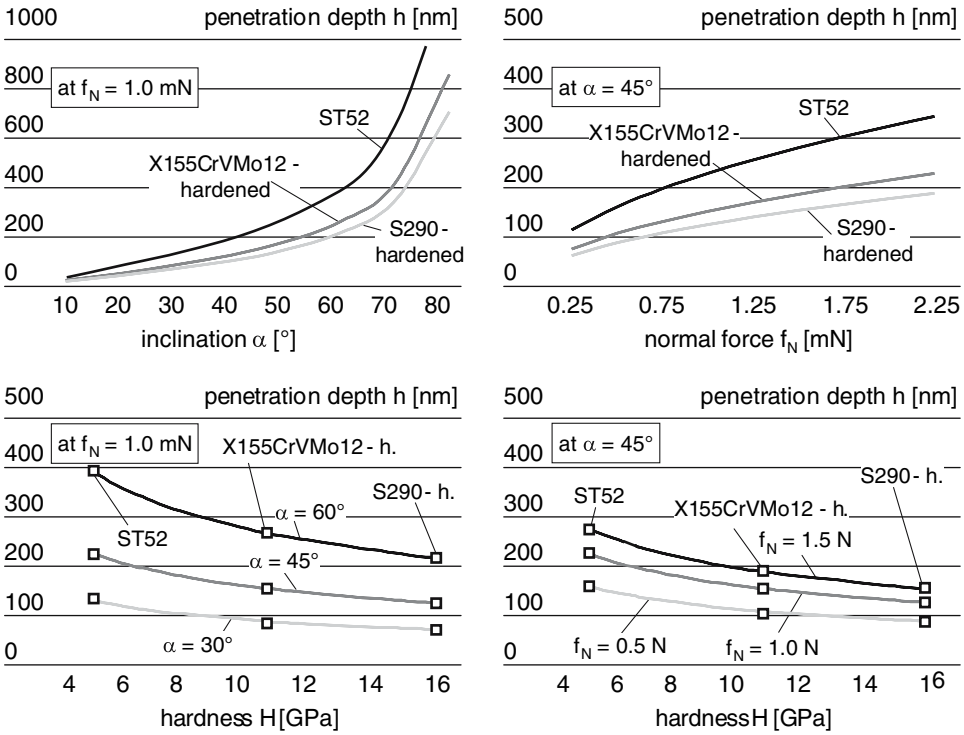

Fig. 5 Penetration depth for different materials in relation to hardness, normal load and inclination

4 Analysis of material stress

During polishing, both the normal load component, responsible for the penetration of the abrasive particle into the workpiece surface, and the tangential load component, responsible for sliding movement or yielding, must be considered. Both load components generate flow stress, which manifests itself in the form of pressure, tension and shearing. This loading leads to elastic and plastic deformation, and to material removal. A matter of particular interest is the relationship between the localized stress and the yielding point and the material fatigue limit respectively. Likewise, a microphysical analysis of the shearing stress in the sliding system and at the points where micro cracks form is important [9]. The plastic deformation and the resulting material hardening changes the mechanical properties in the boundary zone. The occurrence, whether plastic flow will take place by identifying both the stress distribution on the workpiece and the equivalent stress can be determined.

Figure 6 is a schematic diagram of the load transmission conditions. While elastic contact (Hertzian contact) results in elliptical stress distribution, plastic contact leads to a constant pressure distribution. Owing to the ductile material properties of steel and the corresponding material plastification in the contact area, the subsequent analyses are to be based on a constant pressure distribution. Frictional shearing stress is superimposed onto this contact behavior in order to model the dynamic contact due to the

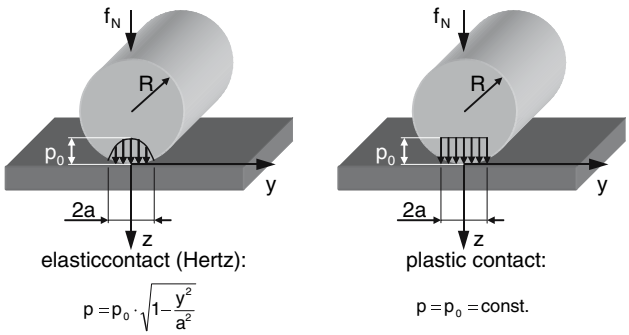

Fig. 6 Schematic diagram of load transmission conditions in cylinder/plane contact model

relative movement between the polishing grain and the workpiece surface. In comparison to purely normal loading under the same conditions, this dynamic model is subject to increased flow stress distributed asymmetrically in both materials.

The calculations carried out in the following stress analyses are based on the Hertzian equation and the described contact geometry model. The stress distribution for a uniform stress state during plastic contact with superimposed frictional shearing can be calculated by equations as provided by Wuttke [9].

Figure 7 shows the curves for the stress components σ_y and σ_z for steel with a Poisson's Ratio of $\nu = 0.3$ under normal loading ($\mu = 0$) and with superimposed normal and tangential load components. The stress and lengths are

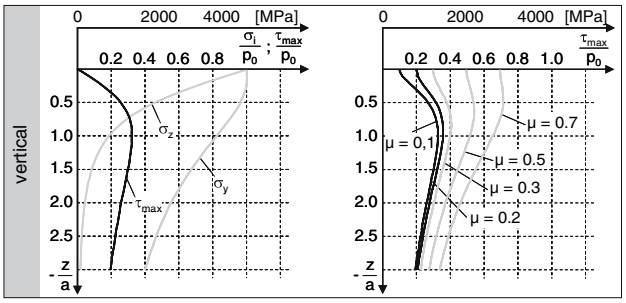

Fig. 7 Stress curve for plastic contact with normal loading (*left*) and with superimposed normal and tangential loading (*right*)

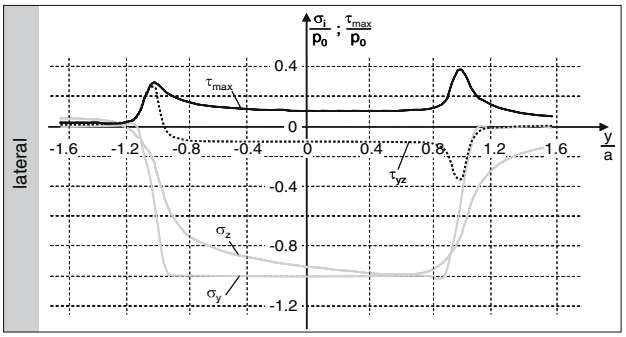

Fig. 8 Stress curve for plastic contact with superimposed normal and tangential loads (depth $z/a = 0.05$, friction coefficient $\mu = 0.1$)

given in relation to p_0 and a. The maximum shearing stress curve is calculated as follows:

$$\tau_{\max} = \sqrt{\left(\frac{\sigma_y - \sigma_z}{2}\right)^2 + \tau_{yz}^2} = k \tag{5}$$

whereby k is the shearing yield stress that is linked experimentally via a uniaxial tensile test according to Tresca's yield criteria to the tensile yield stress σ_F [9]:

$$\sigma_F = 2 \cdot k \tag{6}$$

Considering the curve for maximum shearing stress τ it becomes evident that under purely normal loading, the maximum stress is not found directly in the contact region, but below the surface at a depth of $-z/a = 1.0$ (Fig. 7, left). As friction increases, the point of maximum shearing stress shifts successively to the surface (Fig. 7, right). Regarding the friction load between diamond and steel (with a friction coefficient of 0.1–0.2, according to [10]), the analysis shows that the maximum stress is generated below the surface.

These correlations along with the contact analysis allow a quantitative estimation of the flow stress. The stress generated on the basis of a normal load per grain $f_N = 0.5$ mN is shown in Fig. 7, and can quickly increase to over 1,000 MPa. Only hardened steels with a slightly higher tensile strength have a yield stress in this order of magnitude. The yield stress of non heat-treated steels is lower. This emphasizes the point that the yield conditions can also be achieved in hardened crystal structures when the normal and tangential loads are superimposed. Similarly, half the contact width a was calculated using the Hertzian equation and is included in the diagrams in Fig. 7. In accordance with the diagram, the material loading relevant for material removal during polishing is generated in the first 150 nm below the sliding movement.

By viewing the lateral dimension of the stress curves, the stress exerted on a unit volume of material at a specific depth can be analyzed (Fig. 8). Here, it becomes clear that the stress field is distorted towards the y-axis. Two shearing stress peaks $\tau_{\max}$ can be discerned at $y = a$ and $y = -a$. In other words, when friction is introduced, the maximum load is generated directly in front of and behind the point of contact. Observing stress σ_z, it also becomes clear that transition from compressive stress to tensile stress takes place directly below the surface ($z/a = 0.05$). It is important to bear in mind that hardened crystal structures are particularly susceptible to crack formation, which occurs in the surface area directly behind the point of contact with the polishing grain.

The maximum shearing stress is generated below the surface when subjected to the material loading caused by the polishing grain. The stress peaks would only arise at the surface under friction coefficients higher than given in literature for diamond and metal. Analysis in the lateral dimension shows that the maximum load is experienced directly in front of and behind the polishing grain. Material removal therefore begins at the point of maximum shearing below the surface and continues up to the region directly in front of the polishing grain. The areas behind the polishing grain are also of interest, as they are subject to tensile loading, which can lead to an increased risk of crack formation, particularly in hardened materials. A quantitative analysis of the maximum shearing yield stress clearly shows that the yield stress required for each material is achieved even by very soft polishing pads with embedded polishing grains. It also becomes apparent that the maximum material load which ultimately leads to material removal extends down to a depth of approx. 100 nm. Caution is advised here, since the quantitative analyses do not consider the effects of hardening that occurs due to the polishing grains plowing into the material. This could have a significant effect on the results due to the changes in material properties.

5 Summary and conclusions

In this paper, the contact behavior between the polishing pad and the workpiece surface has been investigated using

a FE model. The calculations showed that the real contact area is about 1% of the apparent contact area. Therefore, high-localized surface pressure occurs that determines the normal force on a single grain, which in its order of magnitude is comparable with nanoindentation processes. Although the investigations were carried out for steel polishing related research, some general conclusions can be drawn. Especially the material properties of the surface zone (up to 300 nm) are relevant and differ from the properties of the underneath material. The material removal mechanism in polishing can be described by the penetration of the abrasive particle into the workpiece surface and a following sliding movement or yielding. The investigations showed that the penetration depth is significantly determined by the inclination of the abrasive particle. An increased hardness or greater normal loads per grain have a relatively small effect. Based on an analysis of the material flow stress using the Hertzian equations it was determined that material removal is initiated at the point of maximum shearing below the surface and continues up to the region directly in front of the polishing grain. Even with soft polishing pads a sufficient amount of yield stress enabling material removal is achieved.

References

1. Klocke F, Hambücker S, Dambon O (2002) Influences exerted by the pad material and polishing suspension on reproducibility of a polishing process. Prod Eng IX/2:51–54
2. Archard JF (1953) The temperature of rubbing surfaces. J Appl Phys 24:981–988
3. Greenwood JA, Tripp JH (1967) The elastic contact of rough spheres. ASME J Appl Mech 34:153
4. Greenwood JA, Williamson JBP (1966) The contact of nominally flat surfaces. Proc Roy Soc Lond A 295:300
5. Qin K, Moudgil B, Park C (2004) A chemical mechanical polishing model incorporating both the chemical and mechanical effects. Thin Solid Films 446:277–286
6. Zhao Y, Chang L (2002) A micro-contact and wear model for chemical–mechanical polishing of silicon wafers. Wear 252:220–226
7. Macosko CW (1994) Rheology—principles, measurements, and applications. VCH, New York
8. Dambon O, Demmer A (2006) Surface interactions in steel polishing for the precision tool making. Ann CIRP (in press)
9. Wuttke W (1986) Tribophysik. VEB-Buchverlag, Leipzig
10. Yurkov AL, Skvortsov VN, Buyanovsky IA, Matvievsky RM (1997) Sliding friction of diamond on steel, sapphire, alumina and fused silica with and without lubrication. J Mater Sci Lett 16:1370–1374